

Protecting a Pd/CB catalyst by a mesoporous silica layer

Tommy Haynes^a, Ovidiu Ersen^b, Vincent Dubois^c, Didier Desmecht^c, Keizo Nakagawa^d, Sophie Hermans^{a,*}



^a IMCN Institute, MOST division, Université catholique de Louvain, 1 Place Louis Pasteur, B-1348 Louvain-la-Neuve, Belgium

^b Institut de Physique et Chimie des Matériaux de Strasbourg (IPCMS), UMR 7504 CNRS – Université de Strasbourg, 23 rue du Loess, BP 43, 67034 Strasbourg Cedex 2, France

^c Department of Physical Chemistry and Catalysis, LABIRIS, 1 avenue Gryson, B-1070 Brussels, Belgium

^d Center for Membrane and Film Technology, Graduate School of Science, Technology and Innovation, Kobe University, Kobe 657-8501, Japan

ARTICLE INFO

Keywords:

Deactivation

Carbon

Mesoporous silica

Glucose oxidation

Palladium

ABSTRACT

Palladium nanoparticles supported on carbon black were encapsulated in a thin mesoporous silica layer. APTES ((3-aminopropyl) trimethoxysilane) was used as anchoring agent to ensure robust and homogeneous formation of a mesoporous SiO_2 layer around the supported catalyst. This was confirmed by XPS, TEM, electron tomography and nitrogen physisorption measurements. The covered catalyst was tested in the oxidative dehydrogenation of glucose into gluconic acid: the high catalytic activity was maintained in comparison with uncovered catalyst, indicating that the underlying active phase was still available. In addition, the silica layer leads to high temperature stability which prevents the agglomeration of palladium nanoparticles upon sintering conditions.

1. Introduction

For many years the production of high-value chemicals from lignocellulosic wood and plant biomass has been a broad area of research [1–3]. Carbon-based compounds derived from biomass are being added as co-feed to fossil fuels towards a sustainable economy. Lignocellulose, which has no nutritional value for humans, is the most abundant raw material on Earth. It contains carbohydrate polymers, cellulose and hemicellulose, and an aromatic polymer, lignin, together with other components such as proteins and fatty acids.

Cellulose is a polysaccharide composed of glucose monomers linked by β -1,4-glycosidic bonds. It can be converted by chemical transformations into valuable substances [4], such as glucose and its derivatives (alcohols and acids) via enzymatic, homogeneous or heterogeneous catalysis. Enzyme biocatalysts for biomass transformations are becoming promising, but as homogeneous catalysts, their recovery after reaction is still a challenge. From this point of view heterogeneous catalysis seems to be the best economical and environmentally friendly alternative for cellulose transformations [4,5].

The conversion of cellulose into useful synthons involves breaking it down to glucose, which is a platform molecule for the synthesis of commercially relevant compounds [2]. For example, glucose oxidation produces gluconic, glucaric and 2-keto-gluconic acids, which are used

in food, pharmaceutical and textile industries. Sorbitol is another example of product arising from glucose by hydrogenation. Sorbitol is widely used as additive in food, cosmetic and paper industries. For all these reasons, transformations of glucose, and namely its selective oxidation in the presence of heterogeneous supported catalysts, have been extensively studied.

Noble metals, especially Pd and Pt, are known to display the highest catalytic activity towards sugar oxidation [6]. Au has also demonstrated its efficiency [7–9]. However, a recurring limitation in heterogeneously catalyzed biomass transformations is deactivation. This loss of activity over time occurs according to various mechanisms such as poisoning, thermal degradation, sintering and leaching [10]. In the case of gold, palladium and platinum catalysts, deactivation can also occur by catalysts over-oxidation [6,11,12]. Supported catalysts are only entering the biomass industry.

Sintering is a particularly important deactivation effect in biomass processing. Most of biomass-based reactions such as hydrolysis, hydrogenations, selective oxidations and dehydrations involve high temperatures and therefore possible sintering [2]. Moreover, a significant number of particle size effects studies have shown that biomass reactions are structure-sensitive [13,14]. Sintering can therefore affect the supported catalyst activity and selectivity. Given the fact that sintering is irreversible for most processes, designing thermally stable catalysts

* Corresponding author.

E-mail address: sophie.hermans@uclouvain.be (S. Hermans).

would make it possible to control, postpone or avoid it. It has been shown that the encapsulation of free-standing metallic nanoparticles in porous oxide materials, i.e. SnO_2 , ZrO_2 and SiO_2 , reduced the deactivation arising from sintering [15–20]. Similarly, one could imagine that such an encapsulation method could also preclude sintering in supported nanoparticles systems. As a matter of fact, two recent examples of covered sinter-resistant Pt supported catalysts are found in the literature [21,22]. Nevertheless, this concept was never explored for particle size dependent biomass transformations. Furthermore, in the referenced examples, no covalent bond exists between the porous encapsulating material and the solid support which could lead to a loss of the protective layer in liquid phase at high temperature [23]. In this context, we have developed a synthesis strategy to covalently coat carbon-supported Pd nanoparticles with a well-structured mesoporous silica layer.

The present work deals with the catalytic oxidative dehydrogenation of glucose into gluconic acid using a carbon black supported-Pd catalyst coated by a covalently tethered SiO_2 shell with mesoporous texture. The chosen carbonaceous material is attractive as palladium support for its non-porous structure which reduces the diffusional limitation risks, as this reaction is carried out in water. Moreover, the carbon black carrier contains some oxygen functional groups that allow grafting of various moieties [24], and will be used here to anchor siliceous compounds. The protective silica layer could represent a potential diffusion barrier for glucose [25]. In order to assess the possible silica layer impact on palladium catalyst activity, a comparison between uncovered and covered catalysts will be made based on normalized activity values (per mmol metal and h^{-1}). The study of Pd nanoparticles resistance against sintering when covered by the silica layer will also be described.

2. Experimental

2.1. Reagents and materials

The carbon black support (CB) was received as 250 G type from IMERYS GRAPHITE & CARBON, while the carbon nanofibers (CNF, LHT type) were supplied by Applied Sciences Inc. (USA). Glucose monohydrate (> 99%), hexadecyltrimethylammonium bromide (CTAB, 95%), sodium borohydride (NaBH_4 , > 98%), (3-aminopropyl) trimethoxysilane (APTES, 99%), tetraethyl orthosilicate (TEOS, > 98%), sodium tetrachloropalladate (II) (Na_2PdCl_4 , 98%), sodium carbonate (Na_2CO_3), and thionyl chloride (SOCl_2 , > 99%) were purchased from Sigma Aldrich and used as received. A commercial ultrasonic cleaner (VWR) was used for sonication.

2.2. Syntheses

2.2.1. Synthesis of Pd/CB catalyst (reference)

A non-covered Pd/CB catalyst used as reference has been synthesized by a conventional precipitation-reduction method [26]: 1 g of CB dispersed in 100 mL of a Na_2CO_3 2.5 wt.% aqueous solution was stirred 15 min at room temperature. 56 mg of Na_2PdCl_4 (corresponding to a theoretical 2.0 wt.% loading) dissolved in 20 mL of distilled water were added dropwise to the suspension within 1 h. 5 g of NaBH_4 diluted in 20 mL of distilled water were then added. The suspension was stirred for 2 h. Finally the catalyst (Pd/CB) was filtered out, washed with distilled water (1 L) and dried overnight at 383 K.

2.2.2. Synthesis of CB-APTES material

2 g of carbon black (CB) were introduced in a 250 mL round-bottom flask containing 100 mL of toluene. 6 mL of SOCl_2 were added and the mixture was heated for 5 h under reflux (393 K). Then, it was filtered out and extensively washed with toluene (500 mL). The resulting material (CB-Cl) was dried overnight under vacuum at 373 K. 1 g of CB-Cl was introduced in a 250 mL round-bottom flask containing 100 mL of

dichloromethane. 1 mL of APTES was added and the mixture was stirred for 24 h at room temperature. Finally, the material (CB-APTES) was filtered out, washed with dichloromethane (250 mL) and methanol (250 mL) and dried overnight under vacuum at 373 K.

2.2.3. Synthesis of Pd/CB-APTES catalyst

A Pd/CB-APTES catalyst was prepared from modified CB-APTES support, using the same synthesis conditions as the reference catalyst above except that a nominal 2.5 wt.% Pd (71 mg Na_2PdCl_4) amount was engaged to counterbalance the dilution effects of the covering layer and so to keep the same wt.% Pd loading.

2.2.4. Synthesis of Pd/CB@ SiO_2 catalyst

0.250 g of Pd/CB-APTES was introduced in a 100 mL round bottom flask containing 25 mL of distilled water. Then 10 mL of NaOH (0.1 M) were added and the mixture was sonicated 10 min. To this suspension 0.571 g of CTAB was added and the solution was heated at 333 K. 0.7 mL of TEOS was added dropwise within 30 min. This suspension was further stirred 3 h 30, then charged into a propylene bottle, which was closed tightly and heated at 373 K for 3 days. The product was filtered out, washed with ethanol (250 mL) and dried at 373 K overnight. The CTAB template was removed by refluxing in ethanol the solid material (Pd/CB@ SiO_2) for 24 h. This procedure can be scaled up to 1 g of starting material.

2.3. Characterizations

The solid catalysts were characterized by X-ray photoelectron spectroscopy (XPS), transmission electron microscopy (TEM), thermogravimetric analysis (TGA), elemental analyses (ICP) and N_2 physisorption.

XPS analyses were carried out at room temperature with a SSI-X-probe (SSX 100/206) photoelectron spectrometer from Surface Science Instruments (USA), equipped with a monochromatized microfocus Al X-ray source. Samples were stuck onto small sample holders with double-face adhesive tape and then placed on an insulating ceramic carousel (Macor[®], Switzerland). Charge effects were avoided by placing a nickel grid above the samples and using a flood gun set at 8 eV. The binding energies were calculated with respect to the C-(C, H) component of the C1s peak fixed at 284.8 eV. Data treatment was performed using the CasaXPS program (Casa Software Ltd., UK). The peaks were decomposed into a sum of Gaussian/Lorentzian (85/15) after subtraction of a Shirley-type baseline.

TEM images were obtained on a LEO 922 Omega Energy Filter Transmission Electron Microscope operating at 120 kV. The samples were suspended in hexane under ultrasonic treatment. A drop of the suspension was deposited on a holey carbon film supported on a copper grid (Holey Carbon Film 300 Mesh Cu, Electron Microscopy Sciences), which was dried overnight under vacuum at room temperature, before introduction in the microscope.

Electron tomography analyses were carried out in the classical TEM mode by using a JEOL 2100F microscope working at 200 kV, equipped with a Cs probe corrector and a GATAN Tridiem imaging filter. For the analyses, the samples were dispersed in ethanol (99.9%) and then a drop of solution was deposited onto a TEM grid covered by a holey carbon membrane. For obtaining the 3D reconstructions, a tilt series in the angular interval of $\pm 75^\circ$ was acquired for the two analyzed samples. The angular increment was set to 1.5° . The tilt series were aligned using the cross-correlation method implemented in the IMOD software. The reconstructions were performed using the SIRT algorithm with 30 iterations, implemented in the Tomo3D software.

Thermograms were recorded on a TGA/SDTA 851e from Mettler Toledo. Samples (5–10 mg) were heated at 10 K/min under a nitrogen flux in alumina containers.

The pore texture of the covered catalysts was characterized by nitrogen adsorption–desorption isotherms. The measures were achieved

by using a Micromeritics ASAP 2020 analyzer at 77 K. Before analysis, the samples (0.02–0.10 g) were degassed for 2 h at 473 K with a heating rate of 10 K/min under 0.133 Pa pressure. The analysis of the isotherms provided specific surface areas calculated with the Brunauer–Emmett–Teller (BET) equation, S_{BET} . The pore volume, V_p , of the samples and the pores average diameter were calculated using the Barrett–Joyner–Halanda (BJH) model.

The elemental analyses (C, H, N, O, Si, Pd) were realized by MEDAC Ltd., UK by microgravimetry for C, H, N, O (direct measure) and by ICP after acid digestion for Si and Pd.

X-ray powder diffraction was carried out by using RINT2500X, Rigaku Corp. with monochromatized Cu $\text{K}\alpha$ radiation at 40 kV and 40 mA.

2.4. Catalytic tests

The oxidation of glucose into gluconic acid was carried out in a 600 mL thermostatized double-walled glass reactor. The pH of the glucose solution was measured continuously by a combined AgCl/Ag Beckman electrode. An automatic titration device Metrohm 842 Titrand was used to neutralize the acids formed over time with a 0.1 M KOH solution to keep the pH at a constant value of 9 during all the reaction. Constant stirring was ensured by a mechanical stirrer (Heidolph RZR 2051 electronic). Oxygen was introduced in the solution under constant flow using a bent glass tube and controlled by a flowmeter. Experimentally, 500 mL of milliQ water were added to the reactor containing 0.9 g of glucose in order to obtain a concentration of 10 mmol/L. When the temperature was set to 323 K, the stirring rate was fixed at 1000 rpm, the oxygen flow at 0.5 mL/min and the pH was brought to 9 with the KOH solution. The catalytic tests are carried out at 50 °C, which is a compromise between: (i) ensuring glucose solubility and (ii) avoiding evaporation of water during the tests. In addition, the rate is much lower at 40 °C, but the results are exactly the same at 50 °C and 60 °C. The test started when the catalyst was added. After 4 h of reaction, the catalyst was recovered by filtration and the filtrate, brought to 1 L, was analyzed by HPLC. HPLC analysis was performed on a Waters system equipped with a refractive index 2414 detector and a UV 2998 Photodiode Array detector. To quantify gluconic acid, an Aminex BioRad HPX-87 C column was used, with CaSO_4 1.2 mmol/L solution as eluent, a flow rate of 0.8 cm³/min, a column temperature of 353 K and 10 μL of injected volume. The gluconic acid yield was calculated using the equation:

$$\text{gluconic acid yield (\%)} = \frac{\text{mmol gluconic acid}}{\text{mmol glucose engaged}} * 100$$

3. Results and discussion

3.1. Pd/CB@SiO₂ preparation

In the first step of catalyst preparation (Fig. 1), carboxylic acid groups existing on the CB (carbon black) surface were chlorinated in refluxing SOCl_2 . After this reaction, the resulting material was reacted with APTES ((3-aminopropyl)triethoxysilane) to produce a robust amide bond [27]. Solid obtained at this intermediate stage is called CB-APTES. The grafting of this silylated precursor was performed to promote the formation of a uniform silica layer onto the catalyst.

Palladium nanoparticles were then deposited on CB-APTES via a precipitation/reduction method using sodium borohydride as reducing agent [26]. Finally the mesoporous silica layer was synthesized by TEOS hydrolysis at 333 K with CTAB as template. In a typical SiO_2 mesoporous material synthesis, CTAB organic template is usually removed by calcination in air [28,29]. Nevertheless, in our case the presence of CB support below the silica layer does not allow the calcination step, which would consume the carbonaceous material. TGA curves of (i) reference 'blank' sample (CTAB deposited on CB) (ii) untreated covered Pd/CB@SiO₂ catalyst, (iii) covered Pd/CB@SiO₂ catalyst treated under air flux as in a typical calcination step (623 K) were recorded, as shown in the Electronic Supplementary Information (ESI 1). The TGA curve of CTAB/CB shows that CTAB is decomposed at ~ 523 K and CB at ~ 948 K. In the untreated catalyst, residual CTAB is clearly confirmed by the mass loss between 473 K and 573 K. In the air-treated catalyst, no CTAB is found but the residual mass is proportionally much higher, indicating that a significant portion of the carbonaceous material had been removed from this sample before TGA analysis. Indeed, TEM images (ESI 2) after this air-treatment show partial combustion of carbon core. To circumvent this calcination step, we decided to wash Pd/CB@SiO₂ in refluxing ethanol to take off the residual template located in the silica pores.

In this study, different synthesis conditions were tested to form the silica coating onto the Pd/CB-APTES catalyst. All these are listed in Table 1. As reported before, the formation of mesoporous silica is strongly influenced by many parameters such as the pH, reaction time and molar ratio CTAB/TEOS [30]. In addition, the incorporation of Pd/CB solid in the reaction mixture for SiO_2 preparation disturbs the synthesis of mesoporous silica, which makes it even more difficult to fine-tune the experimental parameters. All covered samples obtained were imaged by Transmission Electron Microscopy (ESI 3) until optimization. We have noticed that entries 1–5 (Table 1) correspond to experimental conditions engaging too much silica compared to the amount of Pd/CB catalyst implying silica clusters formation onto the CB support. In contrast, in entry 9 the amount of introduced TEOS is too small to cover all the catalyst surface. Moreover, when the reaction time is too short, the produced silica is not well-structured (entries 1–3). As mentioned above, the pH might also have an influence on the silica layer structure. By using more concentrated base solution (entry 8), the silica aggregated and was less uniformly deposited on the CB support. So, the conditions necessary to obtain homogeneously and well-structured silica layer deposited on Pd/CB catalyst are very specific.

The optimal conditions correspond to entry 7. The transmission electron microscopy (TEM) images of this sample are reported in Fig. 2. A comparison with a non-coated Pd/CB material used as reference (see Experimental section) is made in this Figure (Fig. 2a,b). The TEM images of the sample washed by refluxing in ethanol (Fig. 2c, d) indicate clearly the presence of a silica layer uniformly deposited onto the Pd/CB-APTES catalyst. Furthermore, in this sample no silica structure empty of Pd/CB core was observed. It should be noted that scaling up of this procedure could be carried out (we tested up to 1 g of starting Pd/CB-APTES material in one experiment).

To provide further insight on the internal structure of the catalyst grains in terms of morphology and localization of the three distinct phases, we analyzed the 3D reconstructions obtained by electron tomography which avoid the undesirable superposition effect of the different characteristics on the same TEM image. Two typical numerical

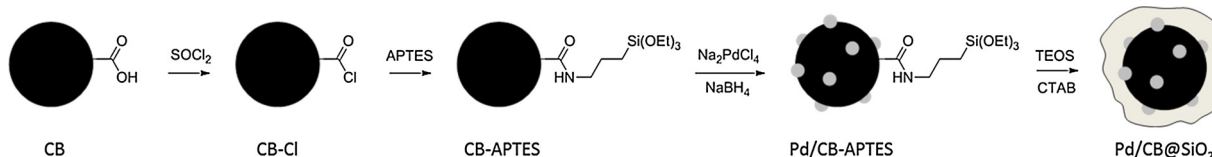


Fig. 1. Synthetic route of Pd/CB@SiO₂ catalyst.

Table 1

Synthesis conditions tested for SiO_2 silica layer formation onto Pd/CB-APTES catalyst.

| Entry | Reaction time (min) | CTAB (g) | TEOS (mL) | TEOS/CTAB molar ratio | NaOH |
|-------|---------------------|----------|-----------|-----------------------|-------|
| 1 | 90 | 3.6 | 4.08 | 1.8 | 0.1 M |
| 2 | 90 | 2.4 | 2.72 | 1.8 | 0.1 M |
| 3 | 90 | 1.9 | 2.72 | 2.3 | 0.1 M |
| 4 | 240 | 1.9 | 2.72 | 2.3 | 0.1 M |
| 5 | 240 | 2.4 | 2.72 | 1.8 | 0.1 M |
| 6 | 240 | 0.9 | 1.00 | 1.8 | 0.1 M |
| 7 | 240 | 0.6 | 0.70 | 2.0 | 0.1 M |
| 8 | 240 | 0.6 | 0.70 | 2.0 | 1.0 M |
| 9 | 240 | 0.4 | 0.50 | 1.8 | 0.1 M |

slices extracted from the reconstruction of the optimized sample, washed by refluxing in ethanol (entry 7) are shown in Fig. 3. The slice-by-slice analysis of the whole volume of the aggregate has shown that the carbon black cores have similar structures as in the case of the uncovered Pd/CB sample and also that all the Pd nanoparticles are localized on the carbon surface. A very important information obtained from this 3D analysis is the fact that the silica covers completely the carbon and the Pd nanoparticles. However, the thickness of the silica shell is not homogeneous as the mesoporous structure fills the voids between the carbon black nodules located in the same aggregate. Another important finding is that mesopores can be observed up to the interface with the carbon as well as at the vicinity of the Pd particles (yellow arrow on the Figure), thus demonstrating the mesoporous character of the whole silica shell and a good accessibility from the outside part of the catalyst aggregate to the Pd active phase.

To confirm i) the anchoring of the silica precursor APTES, ii) the presence of the expected Pd(0) metal and iii) the formation of a silica

layer onto the Pd/CB-APTES catalyst, XPS analyses were realized after each synthesis step for the optimized sample (entry 7 in Table 1). Table 2 shows the atomic percentages of C1s, O1s, N1s, Cl2p, Pd3d and Si2p for each sample. As expected, after covalent APTES anchoring, Si2p surface atomic percentage in CB-APTES material has slightly increased. After the next step, the Pd/CB-APTES catalyst exhibits a Pd3d peak at 335.7 eV corresponding to the binding energy of metallic palladium Pd(0). After the last TEOS hydrolysis step, Si2p surface atomic percentage of covered catalyst (Pd/CB@SiO_2) became higher and conversely, Pd3d atomic percentage decreased. Also, the amount of C diminishes and O increases logically. These results corroborate the silica layer formation on the catalyst. When supported palladium catalyst is coated by a silica layer, the palladium nanoparticles and the carbon black support are covered by a silica matrix, hence are less amenable to surface analysis. A non-optimized sample (entry 8) with the same TEOS/CTAB ratio as optimized sample was also analyzed by XPS. We observe a slight decrease of Pd3d and C1s atomic percentages and, by contrast, a weak increase of atomic percentage for Si2p compared to non-covered Pd/CB-APTES sample. When comparing sample from entries 8 and 7, the amount of deposited Si is lower, hence Pd remains more visible on the surface. These results demonstrated, once more, the high sensitivity of homogeneous silica layer synthesis to the preparation conditions.

The Pd and Si mass percentages in covered catalyst determined by ICP measurements were respectively 0.92 and 10.19 wt.%. The experimental value obtained by ICP for Pd (0.92 wt.%) correlates well with the calculated Pd mass percentage (0.83 wt.%, calculated on the basis of the amount of metallic precursor and silica precursor TEOS engaged in the synthesis) and confirms that the TEOS engaged has almost completely reacted in the selected synthesis conditions.

The Pd/C, Si/C and Pd/Si surface ratios in Pd/CB@SiO_2 catalyst

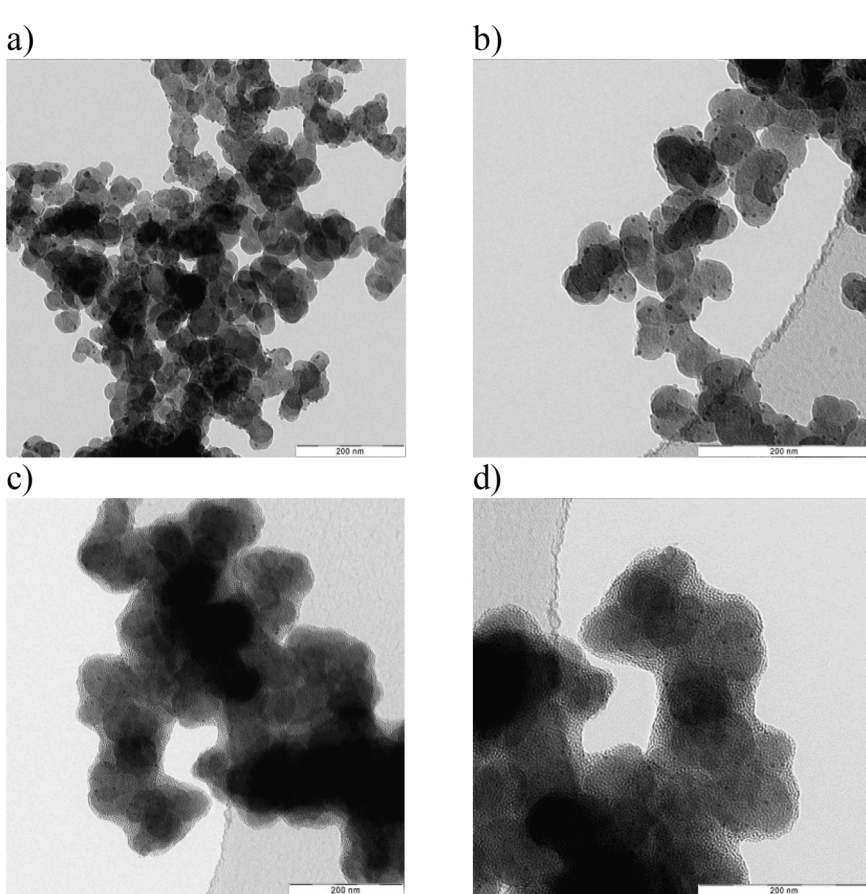


Fig. 2. TEM micrographs of a,b) Pd/CB c,d) Pd/CB@ SiO_2 catalyst washed in refluxing ethanol.

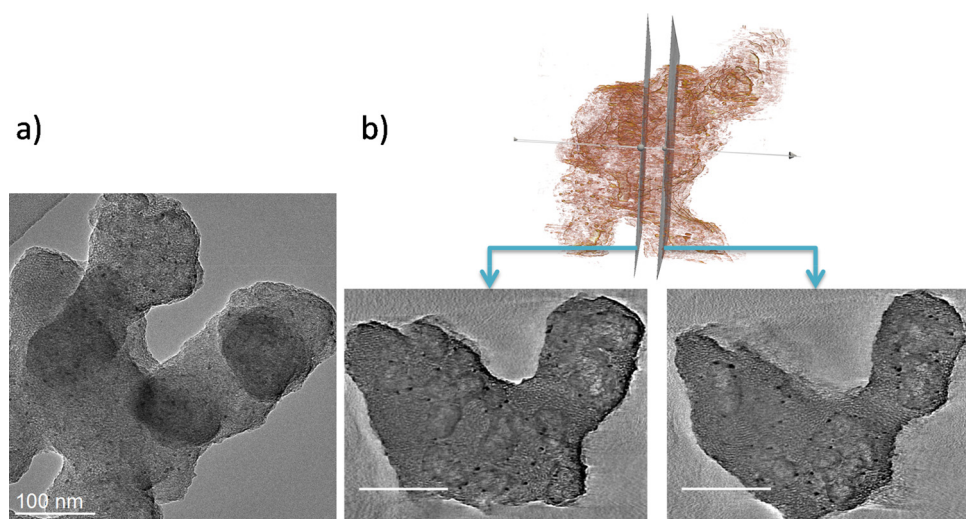


Fig. 3. a) TEM image at 0° tilt from the tilt series used to calculate the volume of the aggregate. b) Two typical numerical slices extracted from the 3D reconstruction. Above, in the middle, the 3D representation highlighting the position of the considered slices.

Table 2
XPS analyses of the materials after each catalyst formation step.

| | CB | CB-Cl | CB-APTES | Pd/CB-APTES | Pd/CB@SiO ₂ (entry 7) | Pd/CB@SiO ₂ (entry 8) |
|------|-------|-------|----------|-------------|-------------------------------------|-------------------------------------|
| C1s | 96.80 | 95.86 | 96.64 | 95.13 | 43.23 | 76.96 |
| O1s | 2.94 | 3.62 | 2.61 | 3.87 | 39.48 | 20.11 |
| N1s | 0.23 | 0.32 | 0.15 | 0.17 | 0.52 | 0.13 |
| Cl2p | / | 0.10 | 0.08 | 0.03 | / | / |
| Pd3d | / | / | / | 0.42 | 0.06 | 0.25 |
| Si2p | / | / | 0.50 | 0.37 | 16.71 | 2.55 |

Table 3
Palladium, silicon and carbon ratios (wt. %) obtained by XPS and ICP for Pd/CB@SiO₂ catalyst.

| | Pd/C | Si/C | Pd/Si |
|------------------|-------|-------|-------|
| XPS ^a | 0.012 | 0.902 | 0.014 |
| ICP | 0.017 | 0.185 | 0.090 |

^a Atomic percentages have been converted into mass percentages.

have also been calculated after XPS analyses and compared with ICP results (Table 3). We note that the Pd/C ratio is higher by ICP analysis than by XPS analysis. This result makes sense, since XPS measurements examine only the catalyst surface. When the silica layer covers the catalyst, not all the palladium present on the catalyst surface is taken into account during XPS measurement while it is measured by ICP analysis. Regarding the Si/C ratio, it is higher by XPS. This again might be explained by the fact that XPS information depth is not sufficient to analyze all the carbon of Pd/CB@SiO₂ catalyst in comparison with ICP elemental bulk analysis. The Si/C ratio estimated by XPS analysis is thus overestimated. Combining both results, it is logical that the Pd/Si ratio is higher in ICP analysis than in XPS measurement. These results prove, again, the formation of a silica layer around the Pd/CB catalyst.

Typical nitrogen adsorption isotherms at 77 K for CB support and Pd/CB@SiO₂ catalysts are shown in Fig. 4. It can be seen that the starting carbon black support exhibits typical nitrogen adsorption-desorption isotherm of non-porous material. In the case of Pd/CB@SiO₂ catalyst, the curve obtained belongs to type IV (according to IUPAC) which is typical for mesoporous materials. Moreover the covered sample possesses an average pore diameter just below 2 nm (ESI 4). The BET surface area and the pore volume obtained after each step of catalyst preparation are summarized in Table 4.

The BET specific surface area of the final Pd/CB@SiO₂ materials is

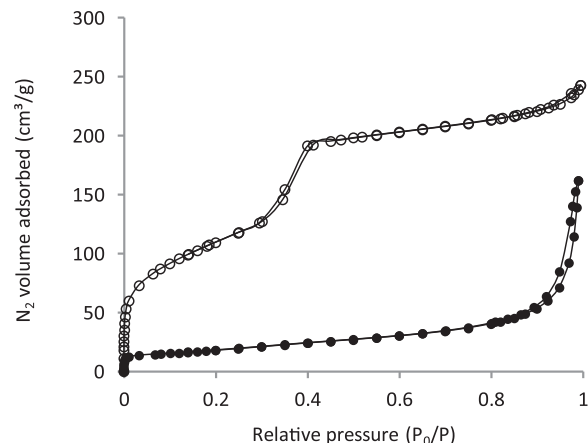


Fig. 4. Nitrogen isotherms at 77 K of (●) starting CB support and (○) Pd/CB@SiO₂ catalyst washed in refluxing ethanol.

Table 4
Textural properties of the solid products isolated after each step of Pd/CB@SiO₂ formation.

| | CB | CB-APTES | Pd/CB-APTES | Pd/CB@SiO ₂ |
|-------------------------------------|------|----------|-------------|------------------------|
| SBET (m ² /g) | 63 | 55 | 56 | 402 |
| V _p (cm ³ /g) | 0.14 | 0.17 | 0.19 | 0.36 |

402 m²/g. These values are much higher than that of starting CB (63 m²/g) and confirm the formation of a porous layer surrounding it. The same trend is observed for pore volume, respectively 0.14 cm³/g for CB and 0.36 cm³/g for Pd/CB@SiO₂. To confirm the mesoporous nature of the protective layer, nitrogen physisorption has been carried out on a CB@SiO₂ material (without Pd) calcined under air to burn off the carbon core (ESI 5). This only-silica calcined sample exhibits an extremely high specific surface area of 1213 m²/g, which is within the typical range of surfaces for mesoporous materials. This increase can be assigned to the total accessibility to the mesopores because the shell is very thin and all pores are open due to carbon removal and also burning off of any residual surfactant. If one take into account the fact that the covered catalysts contain 10.19 wt.% of Si (corresponding to 22 wt.% of silica), with CB surface area unchanged as hypothesis, we calculate that the silica layer could exhibit a specific surface area up to 1830 m²/g. The APTES grafting and Pd nanoparticles deposition steps did not seem

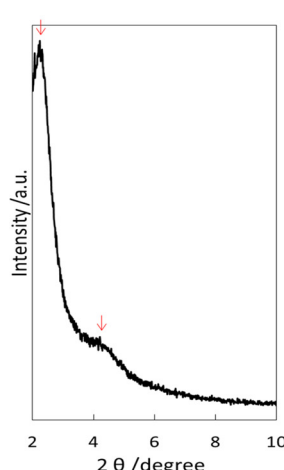


Fig. 5. X-ray diffraction characterization of mesoporous silica layer: peaks are attributed to a mixture of MCM-41 (hexagonal phase) and MCM-48 (cubic phase) [32,33].

to have any influence on the overlayer porosity. These results mean that the surface silica layer homogeneously deposited on Pd/CB catalysts (see Fig. 2c–d) is porous and presents mesoporosity which should allow access to metallic palladium centers underneath it, in agreement with the electron tomography 3D analysis.

In order to assess which mesoporous phase was obtained, the sample was analyzed by powder X-ray diffraction (after burning off the carbon cores by calcination to enhance the signals in the diffractogram). Peaks attributable to MCM-type ordering were found at $2\theta = 2.31$ and 4.33° (Fig. 5). Both MCM-41 and MCM-48 phases (respectively hexagonal and cubic) could contribute to those peaks. It is known that both phases can evolve during hydrothermal synthesis, in the experimental conditions used here, with MCM-41 forming first, then evolving into MCM-48, and ultimately to MCM-50 [31]. Given that the mixture of TEOS and surfactant contain also Pd/CB catalyst, it is to be expected that less perfect crystalline phases are obtained. 3D tomography highlighted the presence of several domains around a single CB aggregate, some with perfectly organized parallel channels (hexagonal phase) and some with interconnected pores (attributable to the cubic phase).

3.2. Catalytic activity

The catalytic performance of the synthesized catalysts was evaluated in biomass model reaction: the oxidative dehydrogenation of glucose into gluconic acid (Fig. 6). The yield in gluconic acid was determined after 4 h of reaction. To determine the influence of the silica layer, catalytic tests were first carried out with reference Pd/CB catalyst without silica coating and a control experiment with the Pd/CB-APTES catalyst. It was shown that APTES grafting did not influence the starting catalytic activity (ESI 6). The comparison between Pd/CB and Pd/CB@SiO₂ was made on the basis of the normalized activity values (per mmol metal and h⁻¹, Table 5). It should be noted that the coating methodology developed in this work does not modify the particle sizes (see Figs. 2 and 9). The palladium mass percentage in the samples is also given in Table 5 and, in order to introduce the same palladium total

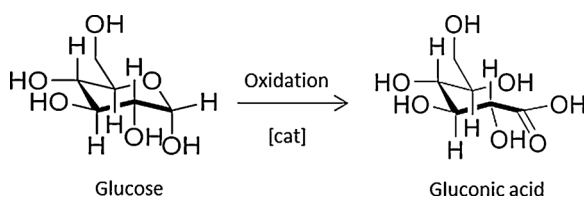


Fig. 6. Oxidative dehydrogenation of glucose.

In case of hexagonal phase

| $2\theta [^\circ]$ | d-spacing | d-spacing ratio (hkl/100) | Theoretical value | hkl |
|--------------------|-----------|---------------------------|-------------------|-----|
| 2.31 | 38.2454 | 1 | 1 | 100 |
| 4.33 | 20.4069 | 0.534 | 0.577 | 110 |

In case of cubic phase

| $2\theta [^\circ]$ | d-spacing | d-spacing ratio (hkl/211) | Theoretical value | hkl |
|--------------------|-----------|---------------------------|-------------------|-----|
| 2.31 | 38.2454 | 1 | 1 | 211 |
| - | - | - | 0.866 | 220 |
| 4.33 | 20.4069 | 0.534 | 0.548 | 332 |

Table 5

Catalytic performance of covered and non-covered palladium catalysts for oxidative dehydrogenation of glucose.

| Sample | Catalyst engaged mass (mg) | Pd mass percentage (%) ^a | Gluconic acid yield (%) | Normalized activity (h ⁻¹) ^b |
|------------------------|----------------------------|-------------------------------------|-------------------------|---|
| Pd/CB | 100 | 2.57 | 34 | 18 |
| Pd/CB@SiO ₂ | 250 | 0.92 | 48 | 28 |

^a Measured by ICP analysis.

^b Normalized activity = (mmol acid gluconic produced)/(mmol Pd *time) [with time = 4 h].

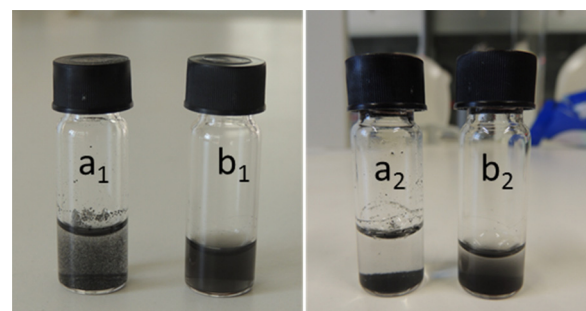


Fig. 7. Dispersion in water of (a) Pd/CB catalyst and (b) Pd/CB@SiO₂ catalyst after (1) 30 min and (2) 4 h.

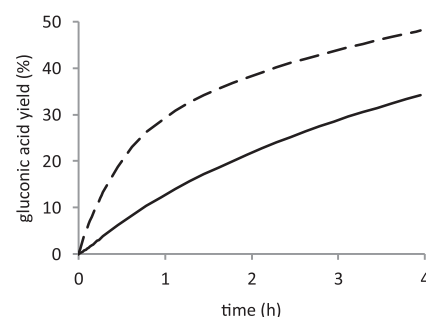


Fig. 8. Gluconic acid yield versus time curves for (—) Pd/CB@SiO₂ catalyst and (—) uncovered Pd/CB catalyst.

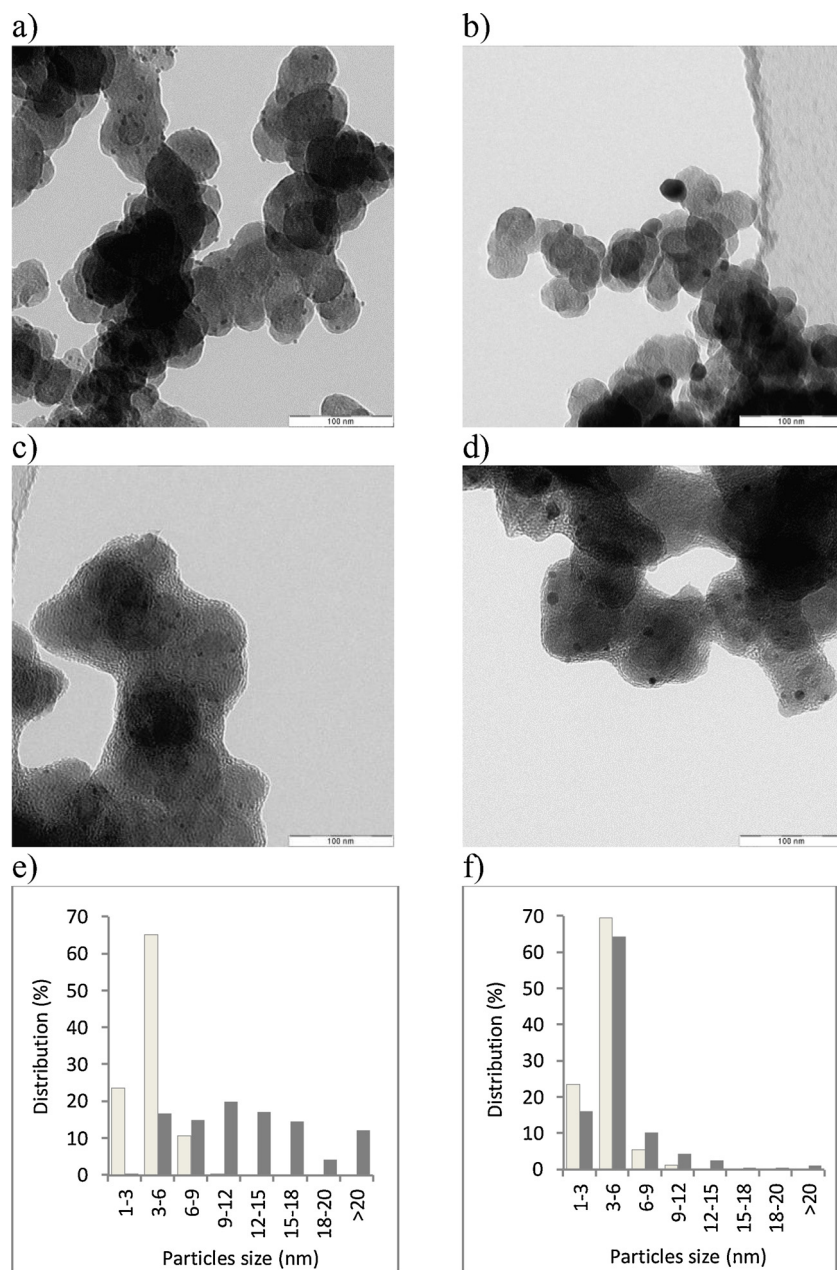


Fig. 9. TEM micrographs of a) Pd/CB b) Pd/CB treated at 873 K d) Pd/CB@SiO₂ and e) Pd/CB@SiO₂ catalyst treated at 873 K. Size distribution of Pd nanoparticles e) in Pd/CB and f) in Pd/CB@SiO₂ untreated (white) and heated (grey) at 873 K.

amount in one catalytic test, the catalyst engaged mass was respectively 100 mg and 250 mg for uncovered and protected catalysts. The normalized activity values obtained for the catalysts, namely 18 mmol gluconic acid*mmol metal⁻¹*h⁻¹ for Pd/CB and 28 mmol gluconic acid*mmol metal⁻¹*h⁻¹ for Pd/CB@SiO₂ are close. The difference observed in normalized activity values between unprotected catalyst and covered catalyst washed in refluxing ethanol could be explained by the catalysts dispersion in aqueous solution. As shown in Fig. 7, the covered catalyst exhibits a better dispersion in water thanks to the hydrophilic silica layer. All these results imply that the pores formed in the SiO₂ sheaths are large enough to allow the crossing of large-size molecules such as glucose in water to reach the Pd metallic centers. Moreover the catalysts exhibit parallel trends over time (Fig. 8) which demonstrates that the silica layer does not modify the glucose conversion mechanism. The covered catalyst could be recovered by filtration and reused in a new catalytic run and was still very active.

3.3. Resistance to sintering

To demonstrate the importance of the mesoporous silica layer to prevent sintering, Pd/CB and Pd/CB@SiO₂ catalyst were heated at 873 K under N₂. The samples were then observed by TEM and Pd particles size distributions were built on no less than two hundred particles. TEM images (Fig. 9a and b) have clearly shown that the resultant particles are sintered in large crystalline aggregates (increasing from 4.0 ± 1.3 nm to 12.3 ± 5.9 nm on average) in the case of the thermally treated non-covered Pd/CB catalyst. Conversely, when the catalyst was encapsulated in the mesoporous SiO₂ layer, the Pd nanoparticles obtained after thermal treatment remained much smaller (before: 4.0 ± 1.3 nm/after: 5.3 ± 3.4 nm). These results imply that the silica layer plays a major role in controlling the size of Pd particles and show the potential of this synthesis approach to reduce deactivation by sintering. Moreover, the S_{BET} obtained after heating the covered

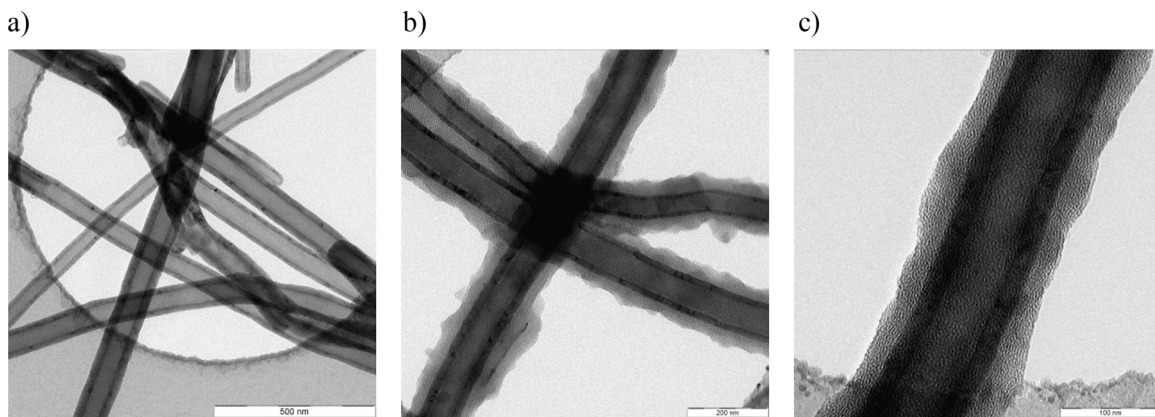


Fig. 10. TEM micrographs of a) bare carbon nanofibers (CNF) and b–c) CNF@SiO₂ coated material.

catalyst does not change significantly (335 m²/g). This also demonstrates that the silica protecting layer retains its structure under harsh thermal conditions, opening the door to demanding gas phase catalytic applications.

The 3D investigation carried out on the thermally treated Pd/CB@SiO₂ catalyst confirms also the findings deduced from the classical TEM and nitrogen sorption measurements. The analysis of the typical slices extracted from the reconstruction volume (See Supplementary Information, ESI 7) demonstrates also that the sintering effect on the Pd nanoparticles is quite limited. When compared to the parameters obtained from the 3D analysis of the initial sample, a slight increase in the particle size can be observed, in agreement with the TEM results, but these particles remain tightly localized at the surface of the carbon black nodules. Though the silica shell and the carbon black are certainly locally affected by the thermal treatment, the silica retains its mesoporous structure and still covers the Pd/CB catalyst.

3.4. Methodology extension

To demonstrate that the methodology developed in this work can be transposed to other forms of carbonaceous supports, carbon nanofibers (CNF) have been covered by a mesoporous silica layer following the same procedure as above. The covered sample (CNF@SiO₂) has been observed by TEM and compared with uncoated CNF (Fig. 10). As can be seen, the silica layer was again uniformly deposited around the CNF (Fig. 10b, c). The starting CNF material presents a S_{BET} specific surface area of 26 m²/g, while it became 158 m²/g after mesoporous silica coating. Therefore these results show clearly that our methodology allows the production of uniformly covered catalysts regardless of the underlying carbonaceous support.

4. Conclusions

In this work, we have demonstrated that by using an aminosilane precursor, a thin mesoporous silica layer can successfully be incorporated onto palladium carbon-supported catalysts. XPS, classical TEM, 3D-TEM by electron tomography and N₂ physisorption confirmed the production of uniform SiO₂ coating on carbon black support. This protected catalyst presented stability at high temperature and resistance to sintering. Moreover, the protected catalyst has retained high catalytic activity towards selective glucose oxidative dehydrogenation, demonstrating the porous nature of silica layer and the accessibility of underlying Pd nanoparticles even in water. The present strategy could easily be extended to other metals, such as Pt and Au, and other carbon supports as demonstrated preliminarily in this work.

Acknowledgements

We acknowledge the FRS-FNRS, Fédération Wallonie-Bruxelles, Loterie Nationale, and Université catholique de Louvain for funding. O.E. acknowledges the financial support of the Institut Universitaire de France (IUF). We are grateful to Jean-François Statsijns for technical assistance, and we also thank the IMERYS GRAPHITE & CARBON firm for generous donation of carbon black and the Applied Sciences firm for providing us with carbon nanofibers.

Appendix A. Supplementary data

Supplementary material related to this article can be found, in the online version, at doi:<https://doi.org/10.1016/j.apcatb.2018.09.018>.

References

- [1] D.Y. Murzin, I.L. Simakova, Catalysis in biomass processing, *Catal. Ind.* 3 (2011) 218–249.
- [2] M. Besson, P. Gallezot, C. Pinel, Conversion of biomass into chemicals over metal catalysts, *Chem. Rev.* 114 (2014) 1827–1870.
- [3] M. Besson, P. Gallezot, Selective oxidation of alcohols and aldehydes on metal catalysts, *Catal. Today* 57 (2000) 127–141.
- [4] H. Kobayashi, T. Komanoya, S.K. Guha, K. Hara, A. Fukuoka, Conversion of cellulose into renewable chemicals by supported metal catalysis, *Appl. Catal. A* 409–410 (2011) 13–20.
- [5] P.L. Dhepe, A. Fukuoka, Cellulose conversion under heterogeneous catalysis, *Chem. Sus. Chem.* 1 (2008) 969–975.
- [6] I.V. Delidovich, O.P. Taran, L.G. Matvienko, A.N. Simonov, I.L. Simakova, A.N. Bobrovskaya, V.N. Parmon, Selective oxidation of glucose over carbon-supported Pd and Pt catalysts, *Catal. Lett.* 140 (2010) 14–21.
- [7] B.T. Kusema, D.Y. Murzin, Catalytic oxidation of rare sugars over gold catalysts, *Catal. Sci. Technol.* 3 (2013) 297.
- [8] S. Biella, L. Prati, M. Rossi, Selective oxidation of D-glucose on gold catalyst, *J. Catal.* 206 (2002) 242–247.
- [9] Y. Cao, X. Liu, S. Iqbal, P.J. Miedziak, J.K. Edwards, R.D. Armstrong, D.J. Morgan, J. Wang, G.J. Hutchings, Base-free oxidation of glucose to gluconic acid using supported gold catalysts, *Catal. Sci. Technol.* 6 (2016) 107–117.
- [10] M.D. Argyle, C.H. Bartholomew, Heterogeneous catalyst deactivation and regeneration: a review, *Focus Catal.* 5 (2015) 145–269.
- [11] M.S. Ide, D.D. Falcone, R.J. Davis, On the deactivation of supported platinum catalysts for selective oxidation of alcohols, *J. Catal.* 311 (2014) 295–305.
- [12] A. Tathod, T. Kane, E.S. Sanil, P.L. Dhepe, Solid base supported metal catalysts for the oxidation and hydrogenation of sugars, *J. Mol. Catal. A Chem.* 388–389 (2014) 90–99.
- [13] N. Meyer, D. Pirson, M. Devillers, S. Hermans, Particle size effects in selective oxidation of lactose with Pd/h-BN catalysts, *Appl. Catal. A* 467 (2013) 463–473.
- [14] C.K. Cheng, P.Y. Xiang, L.C. Jun, Effect of reduction method on the performance of Pd catalysts supported on activated carbon for the selective oxidation of glucose, *Sci. China Chem.* 53 (2010) 1598–1602.
- [15] E. Mine, A. Yamada, Y. Kobayashi, M. Konno, L.M. Liz-Marzán, Direct coating of gold nanoparticles with silica by a seeded polymerization technique, *J. Colloid Interface Sci.* 264 (2003) 385–390.
- [16] S. Ghosh, C.P. Jijil, R.N. Devi, In situ encapsulation of ultra small ceria nanoparticles stable at high temperatures in the channels of mesoporous silica, *Microporous Mesoporous Mater.* 155 (2012) 215–219.
- [17] K. Yu, Z. Wu, Q. Zhao, B. Li, Y. Xie, High-temperature-stable Au@SnO₂ core/shell

supported catalyst for CO oxidation, *J. Phys. Chem. C* 112 (2008) 2244–2247.

[18] I. Lee, Q. Zhang, J. Ge, Y. Yin, F. Zaera, Encapsulation of supported Pt nanoparticles with mesoporous silica for increased catalyst stability, *Nano Res.* 4 (2011) 115–123.

[19] A.J. Forman, J.-N. Park, W. Tang, Y.-S. Hu, G.D. Stucky, E.W. McFarland, Silica-encapsulated Pd nanoparticles as regenerable and sintering-resistant catalyst, *Chem. Cat. Chem.* 2 (2010) 1318–1324.

[20] P.M. Arnal, M. Comotti, F. Schüth, High-temperature-stable catalysts by hollow sphere encapsulation, *Angew. Chem. Int. Ed.* 45 (2006) 8224–8227.

[21] L. Shang, T. Bian, B. Zhang, D. Zhang, L.-Z. Wu, C.-H. Tung, Y. Yin, T. Zhang, Graphene-supported ultrafine metal nanoparticles encapsulated by mesoporous silica: robust catalysts for oxidation and reduction reactions, *Angew. Chem. Int. Ed.* 53 (2014) 250–254.

[22] Y. Dai, B. Lim, Y. Yang, C.M. Cobley, W. Li, E.C. Cho, B. Grayson, P.T. Fanson, C.T. Campbell, Y. Sun, Y. Xia, A sinter-resistant catalytic system based on platinum nanoparticles supported on TiO₂ nanofibers and covered by porous silica, *Angew. Chem. Int. Ed.* 49 (2010) 8165–8168.

[23] H. Xiong, H.N. Pham, A.K. Datye, Hydrothermally stable heterogeneous catalysts for conversion of biorenewables, *Green Chem.* 16 (2014) 4627–4643.

[24] H.P. Boehm, Some aspects of the surface chemistry of carbon blacks and other carbons, *Carbon* 32 (1994) 759–769.

[25] K. Nakagawa, T. Hoshino, K.-I. Sotowa, S. Sugiyama, L. Rkiouak, V. Dubois, S. Hermans, Preparation of Pd nanoparticles covered with organosilica layers and their catalytic properties for cyclohexane dehydrogenation, *Chem. Lett.* 41 (2012) 1308–1310.

[26] T. Haynes, V. Dubois, S. Hermans, Particle size effect in glucose oxidation with Pd/CB catalysts, *Appl. Catal. A Gen.* 542 (2017) 47–54.

[27] J. Li, M.J. Vergne, E.D. Mowles, W.-H. Zhong, D.M. Hercules, C.M. Lukehart, Surface functionalization and characterization of graphitic carbon nanofibers (GCNFs), *Carbon* 43 (2005) 2883–2893.

[28] J. Goworek, A. Kierys, W. Gac, A. Borowka, R.J. Kusak, Thermal degradation of CTAB in as-synthesized MCM-4, *Therm. Anal. Calorim.* 96 (2009) 375–382.

[29] K. Schumacher, M. Grün, K.K. Unger, Novel synthesis of spherical MCM-48, *Microporous Mesoporous Mater.* 27 (1999) 201–206.

[30] I.M. Ortiz, Y.A.P. Mercado, L.A.G. Cerda, J.A.M. Silva, G. Castruita, Influence of the reaction conditions on the thermal stability of mesoporous MCM-48 silica obtained at room temperature, *Ceram. Int.* 40 (2014) 4155–4161.

[31] W.J. Roth, Facile synthesis of the cubic mesoporous material MCM-48. Detailed study of accompanying phase transformations, *Adsorption* 15 (2009) 221–226.

[32] R. Schmidt, M. Stöcker, D. Akporiaye, E. Heggelund Tørstad, A. Olsen, High-resolution electron microscopy and X-ray diffraction studies of MCM-48, *Microporous Mater.* 5 (1995) 1–7.

[33] S.A. El-Safty, T. Hanaoka, F. Mizukami, Large-scale design of cubic Ia3d mesoporous silica monoliths with high order, controlled pores, and hydrothermal stability, *Adv. Mater.* 17 (2005) 47–53.